LBNL-6651E
Date: 26 May 2014

Design Study of the High Luminosity LHC Recombination Dipole (D2)

G. Sabbi and X. Wang

Superconducting Magnet Program, Accelerator and Fusion Research Division
Lawrence Berkeley National Laboratory, Berkeley, CA 94720, U.S.A.

Contents

1 Specifications and design approach 3
2 Initial layout and field error definition 4
3 Yoke frame size and saturation effect 6
4 Coil block positioning and field errors at nominal field 7
4.1 Asymmetric coil layout 8
4.1.1 Impact of individual turns 8
4.1.2 Field error reduction by conductor turn redistribution 9
4.2 Coil block displacement 10
4.2.1 Sensitivity of harmonics to the coil block displacement 10
4.2.2 Field error reduction according to the sensitivities 12
5 Further iteration on the yoke frame 13
6 Roxie-based harmonics reduction 14
7 Comparison to the WP3 field error table version 1.4 16
7.1 Transfer function 16
7.2 Field errors 17
7.2.1 Geometric, saturation and persistent-current effects 17
7.2.2 Random coil block positioning error 18
7.3 Comparison to the error table 18
7.3.1 Systematic errors 18
7.3.2 Random errors 20

8 Fringe field 21
8.1 Yoke OD 560 mm, shell thickness 10 mm 21
8.2 Impact of the yoke OD and shell thickness 22
9 Feasibility of 4.5 T main field 23
9.1 Field errors 23
9.2 Fringe field 25
10 Conclusions 26
11 Appendix: strand and cable parameters 26
12 Appendix: multipole change during coil block design 27
13 References 28

Acknowledgment

This work was supported by the U.S. LHC Accelerator Research Program through U.S. Department of Energy contracts DE-AC02-07CH11359, DEAC02-98CH10886, DE-AC02-05CH11231, and DE-AC02-76SF00515.

Disclaimer

This document was prepared as an account of work sponsored by the United States Government. While this document is believed to contain correct information, neither the United States Government nor any agency thereof, nor the Regents of the University of California, nor any of their employees, makes any warranty, express or implied, or assumes any legal responsibility for the accuracy, completeness, or usefulness of any information, apparatus, product, or process disclosed, or represents that its use would not infringe privately owned rights. Reference herein to any specific commercial product, process, or service by its trade name, trademark, manufacturer, or otherwise, does not necessarily constitute or imply its endorsement, recommendation, or favoring by the United States Government or any agency thereof, or the Regents of the University of California. The views and opinions of authors expressed herein do not necessarily state or reflect those of the United States Government or any agency thereof or the Regents of the University of California.

1 Specifications and design approach

The interaction region layout of the high-luminosity LHC (HL-LHC) requires replacing the recombination dipole magnets (D2) with new ones [De Maria13, Todesco14]. The following baseline specifications were established for the preliminary magnetic design of D2 magnet.

Table 1 Main parameters of the Nb-Ti recombination dipole for HL-LHC [WP3].

Item	Unit	Value
Magnetic length	m	10
Integrated field strength	Tm	35
Aperture	mm	105
Operation temperature	K	1.9
Coil aperture	mm	105
Beam separation	mm	186
Nominal field	T	3.5
Load-line margin	%	30

The dipole field direction is identical in both apertures. The main design challenge is to decouple the magnetic field in the two apertures and ensure good field quality [Todesco14]. The design approach adopted for the recombination dipoles currently installed in LHC [Willen00, Brüning04], using iron yoke as a shield between two apertures, leads to large saturation effects [Gupta13, Todesco13, Todesco14]. A different approach is proposed here, where the iron yoke is designed primarily for low saturation effects, and the resulting large but current-independent cross-talk between apertures is corrected with an asymmetric arrangement of the conductor blocks between the left and right side of each aperture. This method is conceptually similar to the one used in the past for combined function magnets [Nakamoto04], but in this case it is used to cancel the higher order multipolar components rather than introduce them. Full symmetry of the coil and yoke is preserved for the overall twin-aperture magnet with respect to both the horizontal and vertical center lines. The cryostat is concentric with the circular outer surface of the iron yoke. The coil design is based on the LHC dipole cable.

We provide calculations of expected field harmonics for geometric, saturation and persistent current effects, and compare with the error tables used for dynamic aperture studies [Todesco13]. The fringe field as a function of the outer diameter of the iron yoke is also presented. The feasibility of increasing the operating field from 3.5 T to 4.5 T, with a corresponding decrease in magnetic length, is discussed.

The report is arranged as follows. In section 2, an initial coil block layout is presented as the starting point of the analysis and the definition of field errors is given. In section 3, a simple iron yoke geometry is optimized to give an acceptable level of saturation effect. With the selected yoke geometry, the reduction of field errors through asymmetric coil block design is demonstrated in section 4. Due to the dependence of the saturation effect on the coil block layout, a further iteration on the yoke geometry is performed to reduce the b_2 in section 5. With the resulting coil block layout and yoke design, a final optimization of field errors is performed with Roxie and the results are given in section 6. In section 0, the expected field errors are analyzed based on the optimized coil block layout. The contribution from the geometric, saturation, persistent current and random coil block positioning are calculated. The field errors are compared to the latest field error table established for the recombination magnet. In section 8, we discuss the fringe field and perform the parametric study on the impact of the yoke OD and the shell thickness. In

section 9, a prospect of the operation at 4.5 T is discussed in terms of field errors and fringe field. We summarize the major results in section 10.

2 Initial layout and field error definition

In order to assess the potential of the proposed approach, a simplified iron yoke design is used. It has a circular outer surface (OD of 560 mm) and a central window frame characterized by its width and height (Figure 1).

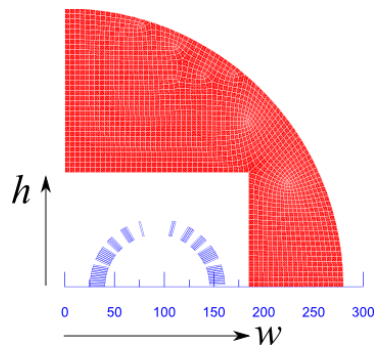

Figure 1 The iron yoke with 560 mm OD and the central window frame (one quadrant is shown). The half width (*w*) and half height (*h*) of the central frame are shown. The top half of the coil blocks in the right aperture are shown.

In addition to the dipole field direction, the magnitude of the main field and field errors must be identical in both apertures (except the opposite signs for the even-order normal harmonics which will be discussed later). Thus, the magnetic field quality will be referred only to the right aperture in this report. The magnetic field in the right aperture can be expressed as a series expansion,

$$B_y + iB_x = \sum_{n=1}^{\infty} C_n \left(\frac{x+iy}{R_{\mathrm{ref}}}\right)^{n-1},$$

where $C_n = B_n + iA_n$ is the complex multipole coefficient in Tesla at the reference radius R_{ref} [Jain98]. B_n is the normal and A_n is the skew coefficient of the multipole field of order n with n =1 corresponding to the dipole field. The field errors are typically normalized to the main field and amplified by a factor of 10000 due to their small amplitude compared to the main field, as given by

$$b_n + ia_n = \frac{B_n + iA_n}{B_1} \times 10^4,$$

where b_n is the normal and a_n is the skew harmonic of order n in units for a dipole magnet.

Analysis was first performed with a 3-block design based on the RHIC dipole cable. At 3.5 T, the preliminary analysis without detailed optimization shows that b_2 can be controlled to 26 units and the low order harmonics up to n = 5 can be controlled to be within ± 5 units, the high-order harmonics are on the order of 10 to 20 units. In addition, the operation point is at 85% of load line at 3.5 T, higher than the desired load-line ratio of 70% due to the reduced iron. Based on this feedback, a 5-block design based on LHC dipole outer layer cable was adopted. The initial 5-block layout as the starting point of the analysis is shown in Figure 2. In each aperture, the coil block has full top-bottom and left-right symmetry. In total, we have 32 cables in each quadrant of one aperture.

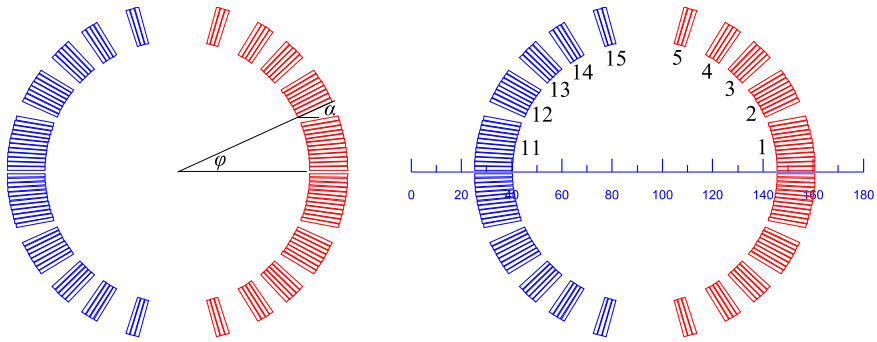

Figure 2 The initial layout of the two apertures with the 5-block design based on the LHC dipole outer layer cable. The polarity of the magnet current is differentiated by the cable color. Block numbers in quadrants 1 (1 – 5) and 2 (11 – 15) in the right aperture are shown. The scale unit is mm.

In addition to the radius, two angles are used to characterize the coil block positioning. One is the positioning angle (φ) and the other is the inclination angle (α), as shown in left aperture in Figure 2. The convention is that the angle increases from the mid-plane to pole, as defined in Roxie [Russenschuck10]. The coil block parameters for the initial layout are given in Table 2.

Table 2 Coil block parameters for the initial 5-block design.

Block	Cable numbers	Positioning angle (degree)	Inclination angle (degree)
1	12	0.546	0
2	8	24.5	24.5
3	5	42.5	42.5
4	4	55.7	55.7
5	3	72.2	72.2

Due to the top-bottom symmetry, the skew harmonics are always zero. With the left-right symmetry with respect to the center vertical line between two apertures, the even order harmonics have the same amplitude but opposite signs between two apertures whereas the odd order harmonics are identical in both apertures.

Nominal current refers to the current with which the nominal dipole field, e.g., 3.5 T, is generated. The injection level is 0.225 T, scaled from the nominal current assuming the injection energy is 450 GeV and the collision energy is 7 TeV.

The field errors for the initial layout are computed at 9500 A at R_{ref} = 35 mm with Roxie. The normal terms in the right aperture are given in Table 3. The normal terms in both apertures have the same amplitude but opposite sign for even-order terms. The skew terms are zero as expected due to the symmetry.

Table 3 The computed normal harmonics in the right aperture at 9500 A, R_{ref} = 35 mm, initial 5-block coil layout. The main field is 3.483 T. The skew terms are all zero.

Harmonics	units
b_2	240.783
b_3	-207.097

Harmonics	units
b_4	36.937
b_5	48.859
b_6	1.841
b_7	6.220
b_8	0.069
b_9	6.082
b_{10}	0.004
b_{11}	-0.559
b_{12}	0.000
b_{13}	0.554
b_{14}	0.000
b_{15}	-0.235

3 Yoke frame size and saturation effect

Using the initial coil block layout, the saturation effect is computed as a function of frame size. Here we define the saturation effect as the difference between the field errors at the nominal field (3.5 T) and the injection level (0.225 T) where the geometric effect dominates. The lower bound of the width and height of the central frame is determined by the coil block and collar size. For the case of LHC 15 mm wide cable (see section 11 for detailed parameters), the coil block reaches 160.5 mm in the mid-plane, which gives the lower bound of 175.5 mm for the half width of the central frame assuming the collar is 15 mm wide. In the vertical direction, the coil block reaches 67.5 mm, which gives the lower bound of 82.5 mm for the half height of the central frame. The upper bound of the central frame size is determined by the mechanical configuration of the magnet cross section. It also affects the load-line ratio and the fringe field as a larger central frame results in less iron available to enhance the central field and return the magnetic flux.

For this analysis we focus on the b_2 and b_3 components as higher-order harmonics and their saturation only depend weakly on the yoke geometries. Figure 3 shows the saturation effect of b_2 and b_3 based on the initial coil configuration. A few patterns can be observed. For a given height of the frame, the saturation of b_2 becomes larger with wider frames. For a given width of the frame, the b_2 saturation decreases with higher frames. These changes are not monotonic as some local minimum can be found (e.g., the small b_2 saturation with w = 180 mm and h = 100 mm). On the other hand, for the same frame size, the saturation of b_3 has a different pattern compared to those of b_2. For example, the b_3 saturation tends to decrease with wider frames. The frame with minimum b_2 saturation does not yield a minimum b_3 simultaneously.

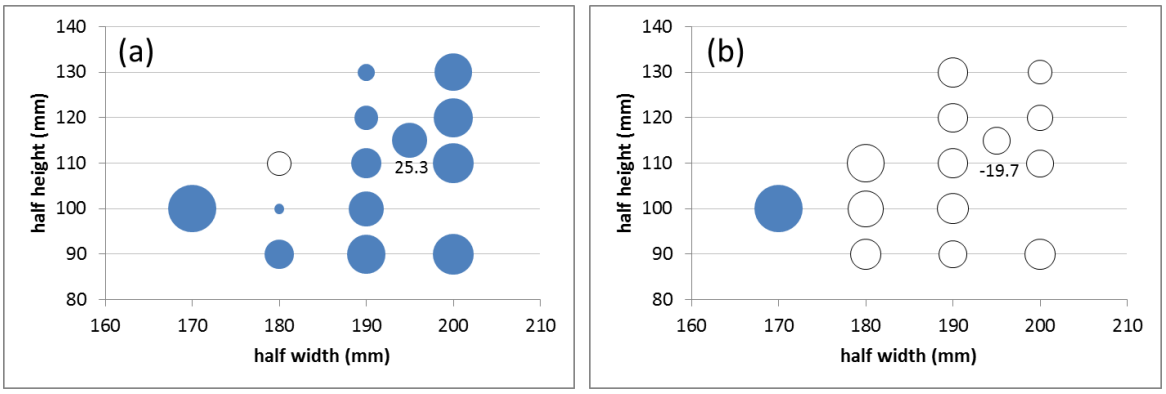

Figure 3 Saturation effect as a function of yoke frame size: (a) b_2 and (b) b_3. The bubble area is proportional to the saturation value. Solid circles correspond to the positive values and open circles correspond to the negative values. The saturation values with w = 195 mm and h = 115 mm are shown. R_{ref} = 35 mm.

The field errors at the nominal field also depend on the size of the yoke frame, as shown in Figure 4. Small harmonics at the nominal field are desirable.

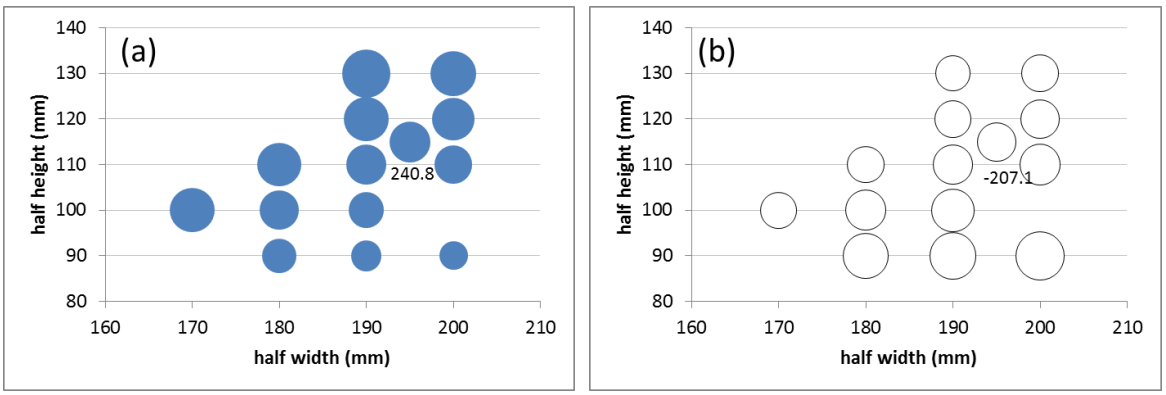

Figure 4 Field errors at the nominal field as a function of yoke frame size: (a) b_2 and (b) b_3. The bubble area is proportional to the field error amplitude. Solid circles correspond to the positive values and open circles correspond to the negative values. The field errors with w = 195 mm and h = 115 mm are shown. R_{ref} = 35 mm.

The following criteria were used to select the yoke frame size: 1) Saturation effect (change of the harmonics level) assuming the harmonics can be corrected by adjusting the coil block positions 2) Harmonics at the nominal field (limited correction by varying block positions) and 3) Sensitivity of harmonics to coil block displacement. Based on this, we select w = 195 mm and h = 115 mm as the initial frame size for the following design iterations.

4 Coil block positioning and field errors at nominal field

A basic coil block design is established as an input for the saturation effect study. With the saturation effect controlled by the iron yoke, coil block positioning is designed to control the field errors at high field. To compensate the large low-order harmonics as shown in Table 3, coil block positioning is adjusted in two steps. The first is to move individual turns from one conductor block to the neighboring one as they transition from the positive to the negative quadrant at the return end. For simplicity of winding and end part fabrication, this shift is limited to a maximum of one turn per block. This operation

leads to an asymmetric coil layout within each aperture, similar to the combined function magnet intended to generate certain low-order harmonics [Nakamoto04] but preserves the overall symmetry with respect to the horizontal and vertical centerlines of the magnet. The second step is to move specific coil blocks to reduce the harmonics due to their linear dependence on the small block displacement which can be shown as part of the sensitivity analysis for dipole magnets [Redaelli00]. A baseline cross section with 5 blocks of LHC cables is presented.

4.1 Asymmetric coil layout

4.1.1 Impact of individual turns

As a first step to optimize the coil layout, we plot the harmonic contribution from each individual turn. For example, if the cable group as shown in Figure 5 is removed (the 1st cable in block 2, or the 13th cable counted from the mid-plane), b_2 in the right aperture will reduce by 50 units. The results for each turn are shown in Figure 6. The red data points correspond to the prime cable in quadrant 1 and the blue data points correspond to primary cable in quadrant 2. Since the amplitudes of field errors are identical in both apertures (except for the sign for even order terms), only the errors in the right aperture are shown.

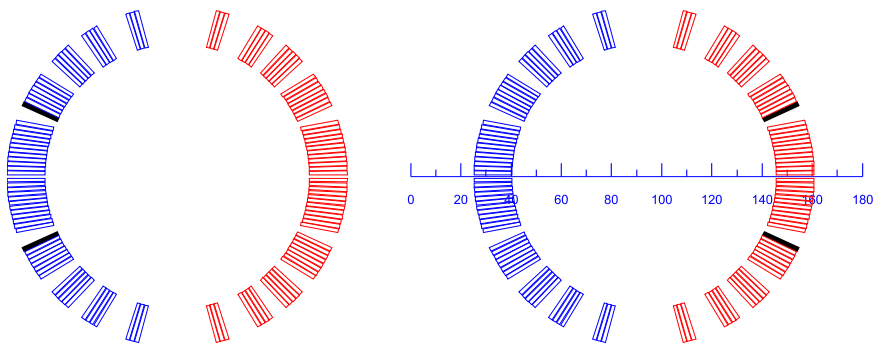

Figure 5 The 1st cable (black cable) removed in block 2 and the associated blocks in the symmetry group are shown as an example.

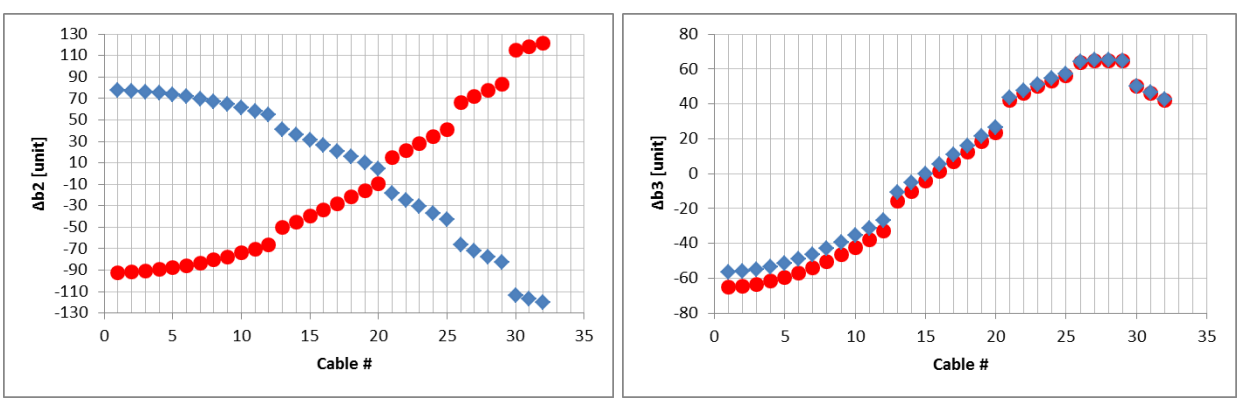

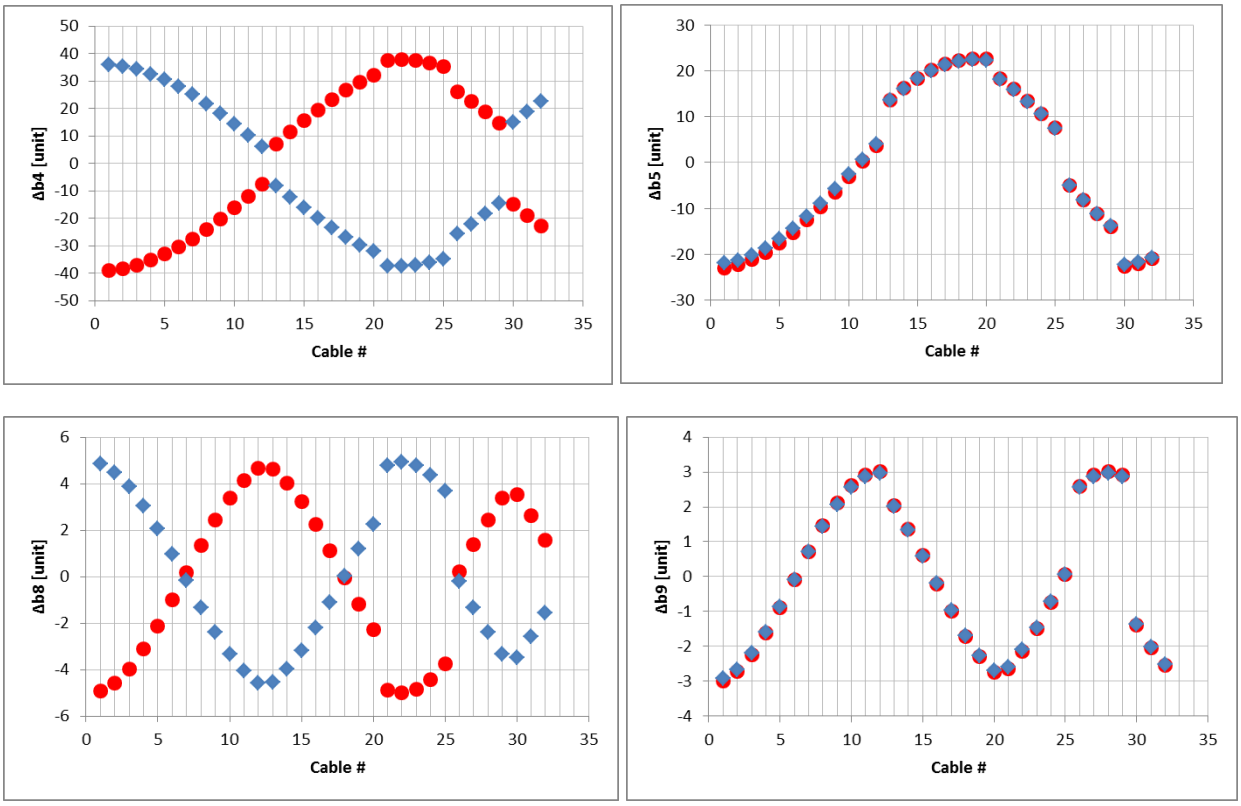

Figure 6 Change in the field errors in the right aperture when one cable group is removed. The red data points correspond to the cables in quadrant 1 of the right aperture and the cables in the associated symmetry groups. The blue data points correspond to the cables in quadrant 2 of the right aperture and the cables in the associated symmetry groups.

The individual turn contributions are different between quadrants 1 and 2 due to the physical distance and cross-talk between two apertures. The difference becomes smaller as the cable moves from the mid-plane toward the pole with reduced coupling of dipole fields from two apertures. The cross-talk in the low-order terms (b_2, b_3 and b_4), in particular for the cables in the mid-plane, is more significant compared to the higher order terms. The contributions from each quadrant tend to cancel each other for the even-order terms, consistent with their non-allowed nature for a dipole magnet with a single aperture.

4.1.2 Field error reduction by conductor turn redistribution

The initial layout features large cross-talk induced field errors from b_2 to b_5 (Table 3). A significant reduction of the resulting harmonics can be obtained through the steps listed below. The block and turn numbers in the steps refer to the right aperture. For each step, the blocks and turns in the left aperture are changed symmetrically.

1. Remove block 11 turn 1 and block 25 turn 3 (the turn is counted from the mid-plane to the pole, same as that of coil block).
2. Remove block 13 turn 5, block 15 turn 1, block 23 turn 5, block 25 turn 1 and other turns following the dipole symmetry. Increased positioning and inclination angles for block 15 from 72.2 degree to 73.97 degree and same for the other 7 blocks following the dipole symmetry in both apertures.

The change in the main field and field errors in the right aperture in each step is listed in Table 4. The main field decreases with less cable turns in each step. Compared to the initial layout, the cross-talk in b_2 and b_3 are reduced by 90%. The reduction in b_4 and b_5 is 40% and 48%, respectively.

Table 4 Change in the main field and field errors in the right aperture in each step. The main field is in T and the field errors are in units with R_{ref} = 35 mm. Transport current is 9500 A for steps.

Step	B_1	b_2	b_3	b_4	b_5	b_6	b_7	b_8	b_9	b_{10}
0	3.48	240.78	-207.10	36.94	48.86	1.84	6.22	0.07	6.08	0.00
1	3.40	31.30	-233.32	22.03	5.87	-13.72	6.45	-6.42	0.68	-0.47
2	3.29	28.93	-16.37	22.82	-25.61	-14.32	4.81	-6.60	-1.99	-0.51

Further reduction in the field errors of various orders would not be as straightforward to achieve by removing more turns. Removing turns to reduce the field error of one order would increase the field error of other orders. At this point, it is more effective to adjust the coil block positioning to further reduce the field errors. The coil block parameters resulted from step 2 are listed in Table 5.

Table 5 Coil block parameters for the first and second quadrant in the right aperture (Figure 2).

Block	Cable numbers	Positioning angle (degree)	Inclination angle (degree)
1	11	2.31	0.9
2	8	24.5	24.5
3	4	42.5	42.5
4	4	55.7	55.7
5	2	73.97	73.97
11	12	0.546	0
12	8	24.5	24.5
13	4	42.5	42.5
14	4	55.7	55.7
15	1	73.97	73.97

The cross section from step 2 gives a main field of 3.53 T with 10300 A. The harmonics are listed in the appendix (section 12). Higher transport current compensates the loss in the main field due to fewer conductors but does not affect the cross-talk.

4.2 Coil block displacement

The coil block positioning can be characterized by three parameters: radius (r), positioning angle (φ), and inclination angle (α). Field errors vary linearly with each of the three parameters if the displacement is rigid and small [Redaelli00]. Based on this principle, we control the field errors by adjusting φ and α as r is fixed for the given aperture. We start from the coil block positioning obtained from step 2 (Table 5). To avoid the skew terms, the coil block displacement follows the top-bottom mirror symmetry.

4.2.1 Sensitivity of harmonics to the coil block displacement

When the change in the coil block positioning follows the dipole symmetry, only the odd-order field errors (allowed terms in a dipole) will be affected. Otherwise, the even-order terms will be affected. It is possible to separate the harmonics into groups with each group affected by one specific displacement (or

step) with minimum cross-talk among groups tuned at different steps, similar to the orthogonal movement principle discussed in [Redaelli00].

4.2.1.1 φ_1 with dipole symmetry

First, we change the positioning angles of block 1 and the associated blocks with dipole symmetry (Figure 7) with $\Delta\varphi_1 = \pm 0.5$ degrees with respect to the nominal value of 2.31 degrees.

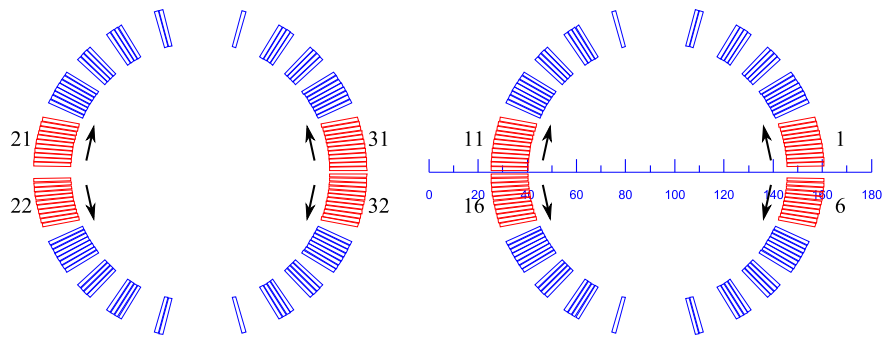

Figure 7 Increase of φ_1 with dipole symmetry. The arrows indicate the direction of the block displacement.

Table 6 gives the resulting harmonics for each φ_1. The odd-order terms are strongly affected and they decrease with increasing φ of block 1 group with dipole symmetry. With 0.5 degrees increase in φ_1, b_3 reduces from -17 units to 1 unit. It is not possible to tune all the harmonics to zero with the change of φ_1 due to different nominal values and sensitivities (slope) for different harmonic orders. Thus, change of the positioning angles for other blocks with dipole symmetry is necessary.

Table 6 Sensitivity of the main field and harmonics to the change of φ_1 with dipole symmetry. All other positioning parameters have the nominal values. The angle is in degree. Main field is in T and harmonics are in units at R_{ref} = 35 mm. Slope is in units/degree.

φ_1	B_1	b_2	b_3	b_4	b_5	b_6	b_7	b_8	b_9	b_{10}
2.81	3.525	26.61	-36.79	22.62	-42.07	-14.40	-3.66	-6.59	-5.36	-0.47
2.31	3.527	27.40	-17.51	22.66	-25.99	-14.49	4.85	-6.67	-2.01	-0.51
1.81	3.529	28.19	1.06	22.75	-10.37	-14.54	13.24	-6.72	1.38	-0.54
Slope	0	-2	-38	0	-32	0	-17	0	-7	0

4.2.1.2 φ_2 without dipole symmetry

To control the even-order terms, we adjust the positioning angle of block 2 and the associated blocks with dipole symmetry. In this case, however, the displacement of each block does not follow the left-right symmetry within each aperture (Figure 8). On the other hand, the left-right symmetry with respect to center line ($x = 0$) and the top-bottom symmetry are preserved.

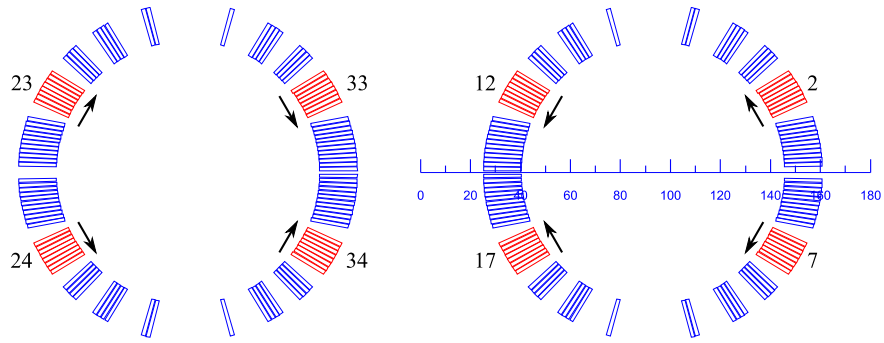

Figure 8 φ_2 increases in blocks 2, 7, 23, and 24 and decreases for the same amount in 12, 17, 33, and 34.

Table 7 gives the sensitivity of the multipoles to three φ_2 values. As expected, only the even-order terms are affected by this displacement. One may simultaneously reduce b_4 and b_8 to zero as shown in Figure 9. For example, this can be achieved with a φ_2 of 25.2 degrees (φ_2 increased by 0.7 degrees in blocks 2, 7, 23, and 24 and decreased by the same amount in blocks 12, 17, 33 and 34).

Table 7 Sensitivity of the main field and harmonics to the change of φ_2 as shown in Figure 8. All other positioning parameters have the nominal values. The angle is in degree. Main field is in T and harmonics are in units at R_{ref} = 35 mm. Slope is in units per degree increase.

φ_2	B_1	b_2	b_3	b_4	b_5	b_6	b_7	b_8	b_9	b_{10}
23.5	3.528	77.25	-16.47	53.93	-24.84	-17.30	5.46	-15.29	-2.10	-3.33
24.5	3.527	27.40	-17.51	22.66	-25.99	-14.49	4.85	-6.67	-2.01	-0.51
25.5	3.526	-22.45	-18.48	-8.61	-25.08	-11.68	5.45	1.96	-2.10	2.31
slope	0	-50	-1	-31	0	3	0	9	0	3

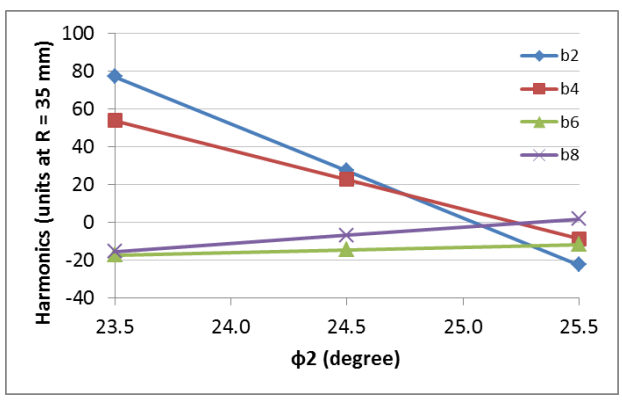

Figure 9 The even-order harmonics as a function of φ_2. At 25.2 degrees, b_4 and b_8 are both zero.

We also see that b_6 and b_{10} are weakly affected, which can be remedied by the displacement in φ_3 that primarily affects b_2 and b_6.

4.2.2 Field error reduction according to the sensitivities

The sensitivity of the harmonics to the positioning and inclination angles of all five blocks can be computed. The main field is not significantly affected because of the small displacement. With the sensitivities, we can perform the following adjustment to reduce the field errors.

3. φ_1 decreases from 2.31 to 1.81 degrees for blocks 1, 6, 21, 22 and decreases from 0.546 to 0.046 degrees for blocks 11, 16, 31, and 32 (dipole symmetry).
4. φ_4 increases from 55.7 to 57 degrees (dipole symmetry).
5. φ_2 increases from 24.5 degrees to 25.2 degrees for blocks 2, 7, 23, 24 and decreases from 24.5 to 23.8 degrees for blocks 12, 17, 33, 34.
6. φ_3 increases from 42.5 to 43.7 degrees for blocks 3, 8, 25, 26 and decreased from 42.5 to 41.3 degrees for blocks 13, 18, 35, 36.

Table 8 Change in the main field and field errors in the right aperture in each step following Table 4. The main field is in T and the field errors are in units with R_{ref} = 35 mm. Transport current is 10300 A for all steps.

Step	B_1	b_2	b_3	b_4	b_5	b_6	b_7	b_8	b_9	b_{10}
3	3.53	28.19	1.06	22.75	-10.37	-14.54	13.24	-6.72	1.38	-0.54
4	3.52	27.79	1.05	22.76	6.51	-14.58	5.00	-6.73	1.21	-0.54
5	3.52	-7.18	0.37	0.82	6.94	-12.61	5.29	-0.67	1.17	1.44
6	3.52	-41.54	0.65	2.63	7.48	0.11	4.81	-1.49	0.95	-1.34

We note that the adjustment listed here is not unique to achieve the minimum field errors. In fact, in step 5, one could reduce b_4 to a negative level such that in step 6, its magnitude can be reduced. A significant increase in the magnitude of b_2 (by a factor of 6) is a tradeoff to reduce b_6.

5 Further iteration on the yoke frame

Since the saturation effect also depends on the field distribution in the yoke, which in turn is affected by the coil design, an iteration on the yoke geometry is performed after the above adjustments in coil block positioning to further reduce the saturation effect. Therefore, the saturation of b_2 and b_3 is studied by varying the yoke geometry around the nominal half width of 115 mm and nominal half height of 195 mm with the following goals: 1) to reduce the b_2 value at high field 2) to maintain the low saturation level for all harmonics, and 3) to maintain the low harmonics at high field. To probe the sensitivity of the harmonics on the yoke size, we vary the yoke size with steps of 5 mm (Figure 10 and Figure 11).

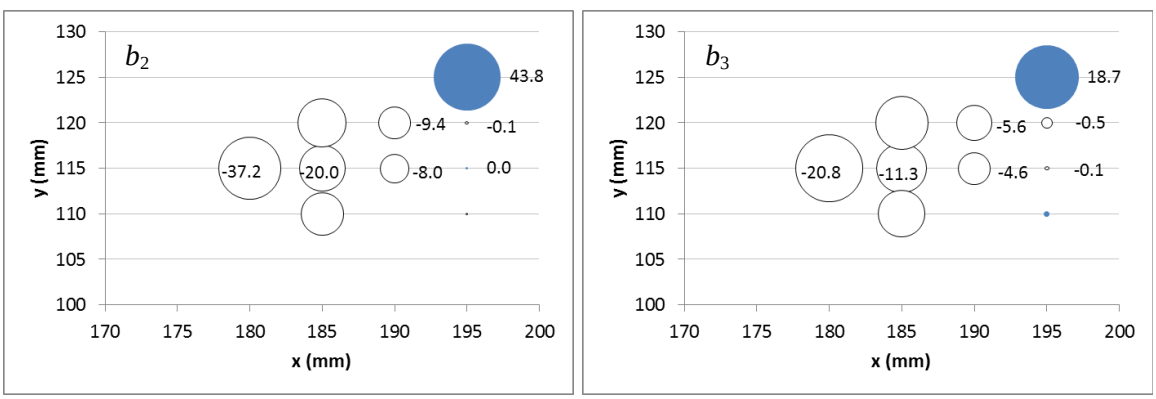

Figure 10 Saturation of the b_2 and b_3 with different yoke geometries between 1150 A and 10300 A.

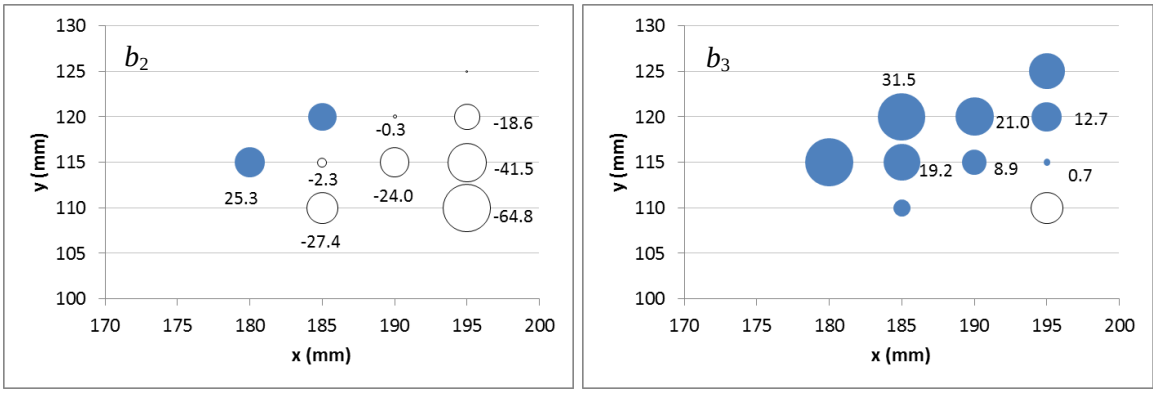

Figure 11 b_2 and b_3 at 10300 A with a main field of 3.5 T. The coil block parameter is given by step 6. R_{ref} = 35 mm.

Two candidate yoke geometries can be identified from Figure 10 and Figure 11: 1) x = 195 mm and y = 120 mm, 2) x = 185 mm and y = 115 mm. The case with x = 190 mm and y = 120 mm is not chosen due to the increased b_3, b_4 and b_5 at 3.5 T compared to the selected cases. Here we use x = 195 mm and y = 120 mm as an example. The change in the yoke reduces b_2 at 3.5 T from -41 units to -19 units (a factor of 2) and increases b_3 from 0.65 units to 13 units (a factor of 20). Other harmonics are not significantly changed. To reduce b_3, one can change the φ_1 with the dipole symmetry as shown in Figure 7 based on the same sensitivity as given in Table 6. The change of the harmonics is shown in Table 9. Step 7 gives the harmonics from the same coil block as in step 6 but with the new yoke size (y is increased from 115 mm to 120 mm). Step 8 gives the harmonics due to the increase of φ_1 from 1.81 degrees to 2.12 degrees ($\Delta\varphi$ = 0.31 degrees) for blocks 1, 6, 21, 22 and increase from 0.046 to 0.356 degrees for blocks 11, 16, 31, and 32 (dipole symmetry). The $\Delta\varphi$ can be determined by minimizing the weighted sum of the odd-order harmonics based on Table 6.

Table 9 Change in the main field and field errors in the right aperture with the new yoke geometry following Table 8. The main field is in T and the field errors are in units with R_{ref} = 35 mm. Transport current is 10300 A for both steps.

Step	B_1	b_2	b_3	b_4	b_5	b_6	b_7	b_8	b_9	b_{10}
7	3.55	-19.20	12.50	2.88	6.70	0.07	4.90	-1.51	0.96	-1.35
8	3.55	-19.73	0.92	2.82	-3.05	0.11	-0.37	-1.48	-1.17	-1.34

The field errors up to n = 15 are compared with those from previous steps in Table 20. In the next section, the coil layout and yoke geometry as in Step 8 will be used as the initial layout for the Roxie optimization.

6 Roxie-based harmonics reduction

The coil block layout from the last step provides the start point for further harmonics reduction based on the optimization routine from Roxie, also taking into account the effect of iron saturation. The Extrem algorithm [Russenschuck10] is used to minimize the objective function $\sum_{n=2}^{12} w_n b_n^2$, where the weighting factors are given as w_2 = 2, w_3 = 5, w_4 = 4, w_5 = 2 and w_n = 3 for n = 6, …, 12. b_n is the normal harmonics at R_{ref} = 35 mm at 3.5 T. The objective functions can be updated with more specific requirements on the field quality from accelerator physics study, e.g., with different weighting factors. Since the field errors

are more sensitive to the positioning angles than to the inclination angles, we vary the poistioning anagles for each coil block in the first and second quadrants in the right aperture (Table 10).

Table 10 The lower and upper bounds for the positioning angles (degrees) of the coil blocks in the first and second quadrants in the right aperture.

φ	Lower bound	Upper bound	Coil blocks
1	1.8	2.5	1, 6, 21, 22
2	0.046	1	11, 16, 31, 32
3	25	27	2, 7, 23, 24
4	23	27	12, 17, 33, 34
5	43	46	3, 8, 25, 26
6	41	44	13, 18, 35, 36
7	56	59	4, 9, 27, 28
8	56	59	14, 19, 37, 38
9	72	80	5, 10, 29, 30
10	72	85	15, 20, 39, 40

The resulting coil blocks are shown in Figure 12 with the parameters listed in Table 11. The resulting field errors will be discussed in Section 7.

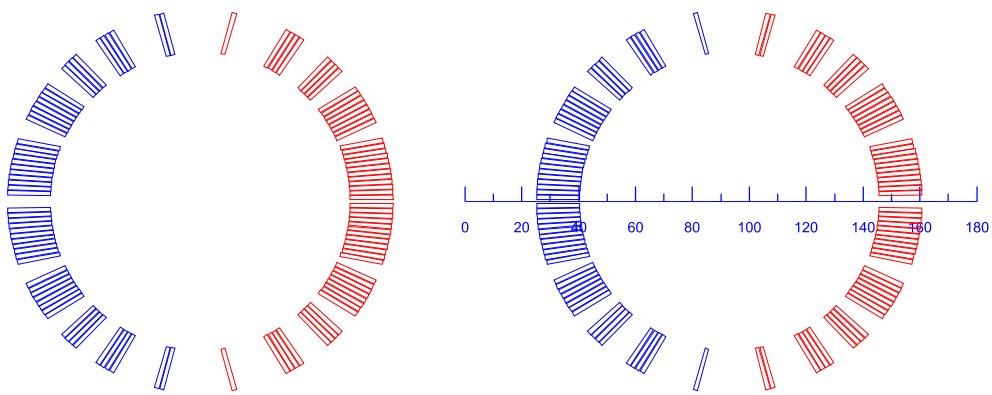

Figure 12 The coil block layout after Roxie optimization. It has the top-bottom symmetry and the left-right symmetry with respect to x = 0. Conductor color indicates the current polarity.

Table 11 Coil block parameters for the first and second quadrant in the right aperture for the Roxie-optimized cross section (Figure 12). The block number definition is given in Figure 2.

Block	Number of cables	Positioning angle (degree)	Inclination angle (degree)
1	11	2.1207	0.9
2	8	25.490	24.5
3	4	44.224	42.5
4	4	57.444	55.7
5	2	76.740	73.97
11	12	0.5584	0
12	8	24.062	24.5
13	4	42.621	42.5
14	4	58.017	55.7
15	1	80.491	73.97

At the nominal current 10500 A, the bore field is 3.521 T and the peak field in the coil is 4.126 T. This gives a ratio of 1.172. The load-line is plotted in Figure 13. The cable critical current as a function of applied field is determined based on the $J_c(B)$ fitting [Bottura02] and strand parameters available in Roxie cable data file. The maximum load line working point is 54%.

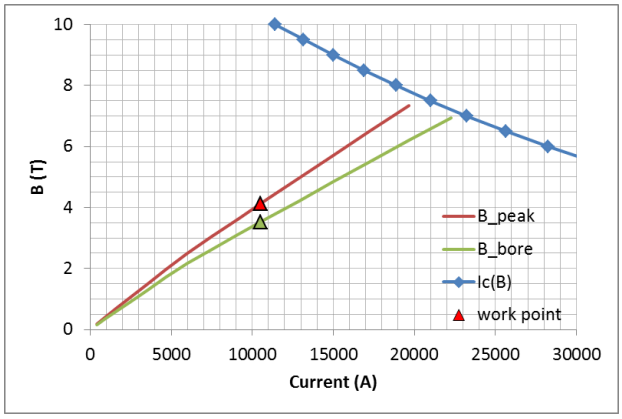

Figure 13 Load line for the coil layout optimized at 3.5 T. The maximum load line working point is 54%.

7 Comparison to the WP3 field error table version 1.4

We evaluate the 2D field quality resulting from the above optimization (Figure 12 and Table 11) and compare it to the WP3 field error table version 1.4, the latest version when this report is completed [Todesco13]. The expected main field and field errors in the magnet straight section are presented considering the geometric, saturation and persistent-current effects. Field errors due to random coil block positioning are also discussed. The nominal current is 10500 A corresponding to a main field of 3.5 T. The minimum current is 50 A. The injection current is 675 A given that the proton center-of-mass energy is 0.45 TeV at the injection and 7 TeV at the collision level per beam.

This persistent-current effect is computed with Roxie which implemented the Nested Ellipse Model [Völlinger02] and the $J_c(B)$ fitting for the LHC dipole outer layer conductor [Bottura02]. The calculation considers a current ramp sequence composed of three segments: the first up-ramp, followed by the down-ramp and the second up-ramp. The first up and down ramps simulate the pre-cycle between the minimum and nominal currents whereas the field errors in the second up-ramp are relevant for the accelerator performance. The persistent-current effect in this report refers to the field errors in the second up-ramp.

7.1 Transfer function

As shown in Figure 14, the low-current transfer function is 0.3681 T/kA. Saturation starts to be significant at about 2900 A. The transfer function reduces by 8.9% at 10500 A (3.5 T). At the injection level, the persistent-current effect during the second up-ramp corresponds to -17 units in the transfer function compared to its geometric value. The persistent-current effect contributes to -0.3 units to the transfer function at 10500 A.

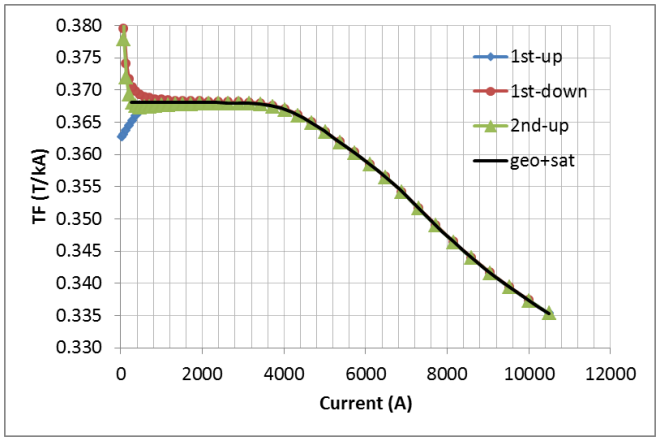

Figure 14 The calculated main field transfer function. The contributions from the geometric, saturation and persistent-current effects are shown.

7.2 Field errors

7.2.1 Geometric, saturation and persistent-current effects

Figure 15 shows the computed low-order field errors (n = 2, …, 5) as a function of current. The geometric effect is defined as the field errors at 100 A from the black data lines shown in Figure 15. Among the field errors up to order n = 15, the top three harmonics with the highest geometric effects are b_4 (2 units), b_3 (1.8 units) and b_{15} (1.5 units). Similar to the main field transfer function, the saturation effect becomes significant around 2900 A. For field errors up to n = 4, the saturation effect increases first followed by a decrease towards the nominal current level, leading to a field-error peak around 6500 A for b_2 and b_3 and 6100 A for b_4. As a result, the variation is 14 units for b_2, 7 units for b_3 and 3 units for b_4, even though they are less than 0.5 units at the nominal current level (Table 13). It remains to be clarified how the non-monotonic variation of b_2, b_3 and b_4 impacts the beam dynamics.

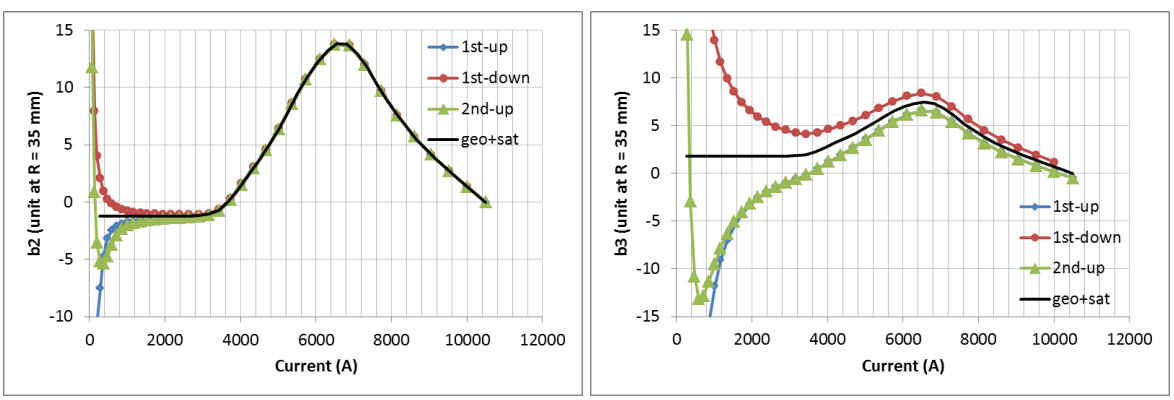

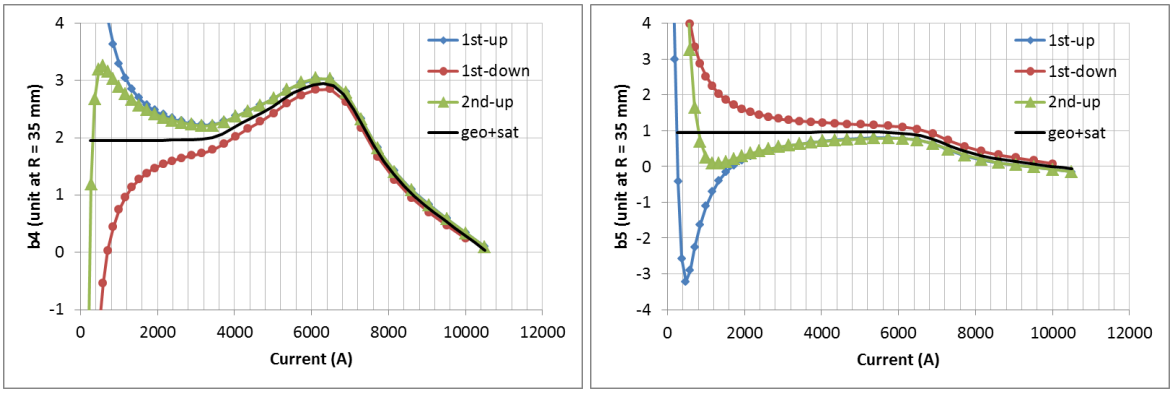

Figure 15 The calculated low-order field errors (n = 2, …, 5) as a function of current.

The persistent-current effects below 2 kA are higher than 1 unit for low-order harmonics up to decapole (n = 5). For higher orders, the effect is less than 0.5 units. Like the geometric and saturation effects, persistent-current effect is expected in both odd- and even-order normal harmonics due to the cross-talk between two apertures and the asymmetric coil layout in each aperture. The effect at the injection level is given in Table 13.

7.2.2 Random coil block positioning error

The field errors due to random coil block positioning error are computed using Roxie. Each of the 40 coil blocks in two apertures is randomly displaced assuming a positioning tolerance d. In total 500 cases are generated and the standard deviation of the field errors from each aperture in each case is calculated. The calculation is repeated for different values of the positioning tolerance. The standard deviation of the field errors can be fitted to the following function $\sigma(d) = d\alpha\beta^n\gamma^{n^2}$, where α, β, and γ are fitting constants [Ferracin00]. For each computation, each of the 40 coil blocks in two apertures is randomly displaced simultaneously. The fitting constants are averaged between two apertures and listed in Table 12. The averaged fitting constants can be used to characterize the random field errors for d between 10 and 100 μm.

Table 12 Fitting parameters for the random multipoles generated by random displacement of the coil block.

d	α	β	γ
[μm]	[1/μm]	[-]	[-]
100	0.115609	0.719383	0.994748
50	0.115604	0.719383	0.994748
30	0.115586	0.719317	0.994752
10	0.115625	0.719326	0.994749
average	0.115606	0.719352	0.994749

7.3 Comparison to the error table

7.3.1 Systematic errors

The normal harmonics are compared to the latest field error table established for D2 magnet version 1.4 [Todesco13] in terms of the contribution from geometric, saturation, persistent current effects. The total

field errors at the injection and high-field levels are also given. The numbers in the parenthesis are from the error table. Only the normal harmonics are considered as all the systematic skew terms are zero due to the symmetry.

Table 13 Comparison between the computed normal harmonics in units from the coil design reported here and the field error table version 1.4 in parenthesis [Todesco13]. R_{ref} = 35 mm.

b_n	Geometric	Saturation	Persistent	Injection	High Field 3.5 T w/o p.c.	High Field 3.5 T w/ p.c.
2	-1.250 (0.000)	1.246 (25.000)	-1.905 (0.000)	-3.154 (0.000)	-0.004 (25.000)	0.009
3	1.771 (18.000)	-1.757 (-15.000)	-14.683 (-14.200)	-12.912 (3.800)	0.014 (3.000)	-0.476
4	1.957 (-8.000)	-1.916 (10.000)	1.233 (0.000)	3.189 (-8.000)	0.041 (2.000)	0.094
5	0.943 (4.000)	-1.012 (-5.000)	1.203 (-1.000)	2.146 (3.000)	-0.069 (-1.000)	-0.150
6	0.336 (0.000)	-0.367 (0.000)	-0.210 (0.000)	0.126 (0.000)	-0.031 (0.000)	-0.018
7	0.191 (0.800)	-0.091 (-1.000)	-0.005 (-0.700)	0.186 (0.100)	0.100 (-0.200)	0.071
8	0.180 (0.000)	-0.006 (0.000)	0.106 (0.000)	0.286 (0.000)	0.174 (0.000)	0.184
9	-0.424 (0.000)	-0.045 (0.090)	0.043 (0.020)	-0.381 (0.020)	-0.469 (0.090)	-0.475
10	-0.249 (0.000)	-0.025 (0.000)	-0.174 (0.000)	-0.423 (0.000)	-0.274 (0.000)	-0.274
11	1.282 (0.000)	0.125 (0.030)	0.149 (0.000)	1.431 (0.000)	1.407 (0.030)	1.408
12	-1.375 (0.000)	-0.134 (0.000)	-0.006 (0.000)	-1.381 (0.000)	-1.509 (0.000)	-1.508
13	0.535 (0.000)	0.052 (0.000)	-0.082 (0.000)	0.453 (0.000)	0.588 (0.000)	0.586
14	0.089 (0.000)	0.009 (0.000)	-0.021 (0.000)	0.068 (0.000)	0.098 (0.000)	0.098
15	-1.446 (0.000)	-0.141 (0.000)	-0.069 (0.000)	-1.515 (0.000)	-1.587 (0.000)	-1.589

The geometric values are given by the harmonics at 100 A without including the persistent-current current effect. The quadrupole term (b_2) is -1.25 units compared to the specified zero value. The sextupole, octupole and decopole are all lower than the levels from the error table. For $n > 7$, the amplitudes of the field errors are less than 0.55 units, except for n = 11, 12, and 15 where the amplitudes of the field errors are less than 1.5 units. The amplitude of these high-order terms would decrease fast with reduced reference radius [$\propto \left(\frac{R}{R_{ref}}\right)^{n-1}$].

For the saturation effect, the underscored numbers indicate the non-monotonic behavior of the saturation curves and the saturation effect here is defined as the difference between the high-field and the geometric values, i.e., the peak levels around 6 kA are neglected for the n = 2, …, 5 (Figure 15). In this case, the saturation effect are well below the limits specified in the error table for n = 2, …, 5. For the high-order terms, the saturation effect is less than 0.37 units.

The persistent-current effect is the difference between the harmonics at the injection level (675 A) and the geometric values. The harmonics are linearly interpolated between two current steps, 588 A and 715 A. The even-order normal terms are allowed in D2 due to the asymmetric coil layout and the cross-talk between the two apertures. This also leads to non-zero even-order persistent-current terms [Sabbi13]. The most significant one is b_2 with 2 units of contribution from the persistent current. The persistent-current effect of b_3 is close to the specified level in the error table (-14.7 units vs. -14.2 units). With the smaller geometric value, however, the persistent-current effect is less compensated which leads to a higher b_3 at

the injection level compared to the value in the field error table. The high-order persistent-current field errors are less than -0.2 units. The contribution from the persistent-current effect is not negligible for the low-order terms ($n \leq 5$), in particular b_3, but is negligible for high-order terms where the geometric effect dominates.

For the field errors at high-field, two columns are included, one with and one without the persistent-current effect. The low-order harmonics ($n \leq 5$) are all significantly lower than the levels specified in the error table. For higher orders, the field errors are dominated by the geometric terms.

7.3.2 Random errors

Table 14, Table 15 and Figure 16 compare the random errors calculated above with those in the present WP3 D2 table (version 1.4) [Todesco13]. A uniform RMS displacement of 30 μm is used for both normal and skew terms of even and odd orders for the asymmetric coil layout in this report.

Table 14 Comparison of the random errors (normal) in units. R_{ref} = 35 mm.

	Error table version 1.4		This report	
Normal	Injection	High Field	Injection	High Field
2	0.200	2.500	1.757	1.757
3	0.727	1.500	1.231	1.231
4	0.126	0.200	0.854	0.854
5	0.365	0.500	0.586	0.586
6	0.060	0.060	0.398	0.398
7	0.165	0.165	0.267	0.267
8	0.027	0.027	0.178	0.178
9	0.065	0.065	0.117	0.117
10	0.008	0.008	0.076	0.076
11	0.019	0.019	0.049	0.049
12	0.003	0.003	0.031	0.031
13	0.006	0.006	0.020	0.020
14	0.001	0.001	0.012	0.012
15	0.002	0.002	0.008	0.008

Table 15 Comparison of the random errors (skew) in units. R_{ref} = 35 mm.

	Error table version 1.4		This report	
Skew	Injection	High Field	Injection	High Field
2	0.679	0.679	1.757	1.757
3	0.282	0.282	1.231	1.231
4	0.444	0.444	0.854	0.854
5	0.152	0.152	0.586	0.586
6	0.176	0.176	0.398	0.398
7	0.057	0.057	0.267	0.267
8	0.061	0.061	0.178	0.178

	Error table version 1.4		This report	
Skew	Injection	High Field	Injection	High Field
9	0.020	0.020	0.117	0.117
10	0.025	0.025	0.076	0.076
11	0.007	0.007	0.049	0.049
12	0.008	0.008	0.031	0.031
13	0.002	0.002	0.020	0.020
14	0.003	0.003	0.012	0.012
15	0.001	0.001	0.008	0.008

For the WP3 table, a symmetric coil layout was used and various assumptions were made in terms of determining RMS displacement for specific order of normal and skew harmonics [Bellesia06], and scaling of random errors taking into account the systematic values for the corresponding components. The random errors we provide in this report are intended as a first assessment of the asymmetric coil layout, but additional work is required to incorporate this information in the official field quality table.

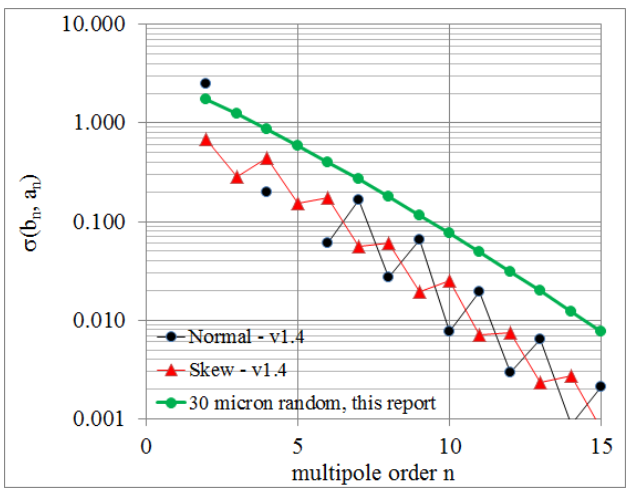

Figure 16 Comparison of the random errors in units between WP3 error table (version 1.4) [Todesco13] and this report. A uniform RMS displacement of 30 μm is used for both normal and skew terms of even and odd orders for the asymmetric coil layout in this report. R_{ref} = 35 mm.

8 Fringe field

The fringe field is considered with the main field at 3.5 T based on the coil block layout. The outer radius of the shell is fixed at 500 mm. The fringe field is computed with Roxie at a radius of 501 mm for comparison with a target level of 20 mT. The fringe field with a typical yoke OD (560 mm) and shell thickness (10 mm) is first presented, followed by the dependence on yoke OD and shell thickness.

8.1 Yoke OD 560 mm, shell thickness 10 mm

There are no rigid requirements for the maximum fringe field in LHC magnets. A general guideline of 20 mT at the surface of the cryostat can be used as an initial target, but higher values can be accepted depending on the local conditions (nearby installed equipment, etc). With a yoke OD of 560 mm and a

cryostat shell thickness of 10 mm at 500 mm radius, the fringe field at the surface of the cryostat (R = 501 mm) ranges from 24 mT to 55 mT with the main field at 3.5 T. This is above the desired 20 mT level but consistent with the expected fringe field in other HL-LHC magnets (e.g. QXF).

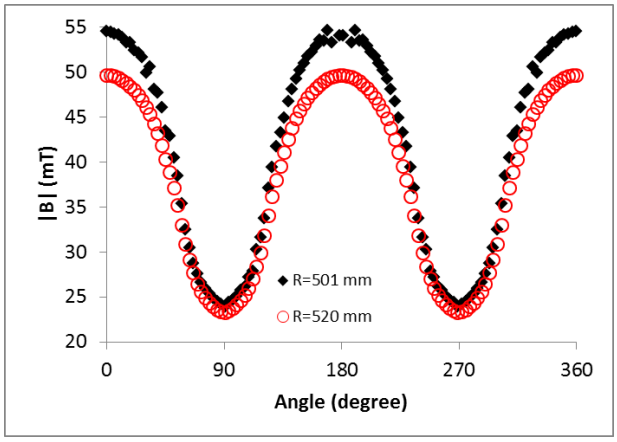

Figure 17 Fringe field with the main field of 3.5 T. Yoke OD = 560 mm, shell thickness = 10 mm.

8.2 Impact of the yoke OD and shell thickness

The fringe field decreases with larger yoke OD and/or thicker shells. As an example, Figure 18 gives the fringe field at R = 501 mm for yoke OD from 560 mm to 600 mm with the 20 mm shell thickness and 3.5 T main field. The magnet current is reduced in the calculation for each case with more iron to maintain the same main field. A simple linear relationship exists between the peak fringe field and yoke OD. The yoke OD would be about 592 mm for the fringe field to be less than 20 mT at a radius of 501 mm. This is consistent with the limits on yoke size established for other HL-LHC magnets (e.g. QXF).

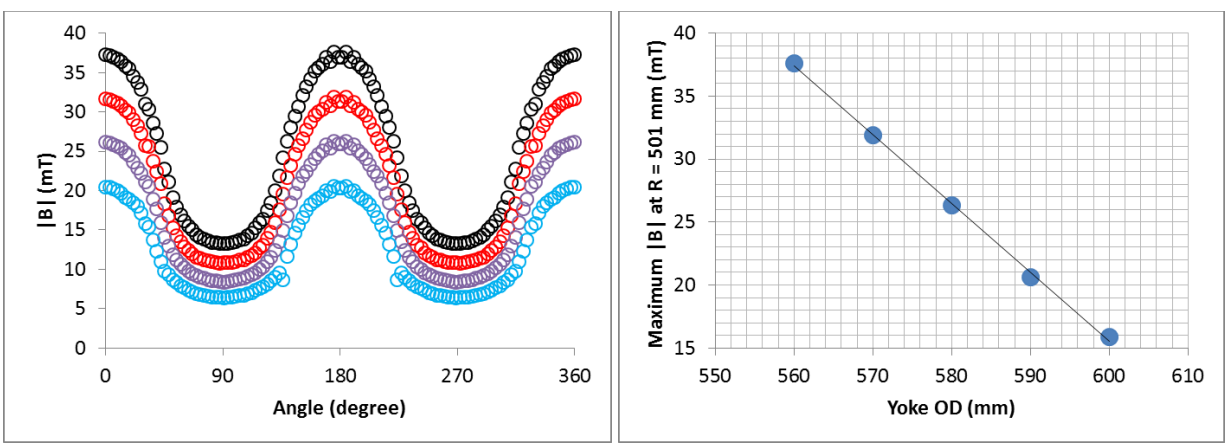

Figure 18 Fringe field at R = 501 mm with different yoke OD. The shell thickness is 20 mm and the main field is 3.5 T. Left: Fringe field at R = 501 mm with the yoke OD increases from 560 mm to 590 mm with steps of 10 mm. Right: Peak fringe field at R = 501 mm as a function of yoke OD.

A parametric study is performed by varying the iron yoke outer diameter and the shell thickness to determine their impact on the fringe field. Linear relationship between the maximum fringe field and yoke OD is observed for several shell thickness ranging from 10 mm to 40 mm. The averaged sensitivity is about -0.51 mT/mm.

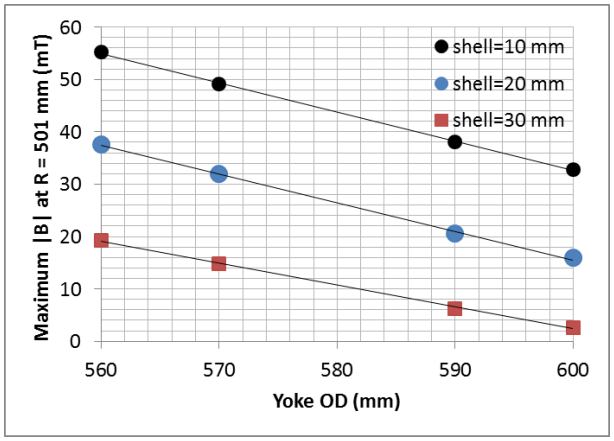

Figure 19 Maximum fringe field at R = 501 mm with different shell thickness and yoke OD with main field of 3.5 T. Solid lines are linear fits of the data points.

The peak fringe field occurs around the mid-plane area (0 and 180 degrees), as expected from the dipole field distribution. Thus, it may be possible to locally increase the thickness of shielding for either the yoke or the outer shell. More in general, a yoke optimization beyond the simple window-frame considered for this study is expected to yield improved performance in terms of maximum field/operating margin, field quality and fringe field characteristics.

9 Feasibility of 4.5 T main field

The current block layout yields a maximum load-line ratio of 54% at 3.5 T. At 4.5 T, the maximum load-line increases to 70%. A main field of 4.5 T reduces the magnetic length from 10 m to 7.8 m while still maintaining sufficient operational margin. In this section, we briefly review the field errors based on the existing coil block design and the fringe field at 4.5 T.

9.1 Field errors

By increasing the current, the field errors, in particular $n \leq 6$, increase compared to the field errors at 3.5 T, but this can be corrected by performing the cross-section optimization at the higher field level. The high-order terms are less sensitive to higher current. An example from the optimization at 4.5 T is given in Table 16 where we compare the main field and field errors between layout 1 optimized at 3.5 T and layout 2 optimized at 4.5 T (with a nominal current of 13850 A). For layout 1, the field errors at 4.5 T are also shown. The field errors of layout 2 at 4.5 T are smaller to those from layout 1 at 3.5 T for $n \leq 6$ and are comparable for higher order terms.

Table 16 Field errors in units with yoke OD = 560 mm and shell thickness of 10 mm. R_{ref} = 35 mm. Coil block layout 1 is optimized at 3.5 T and layout 2 is optimized at 4.5 T.

	Layout 1		Layout 2
B_1	3.5 T	4.5 T	4.5 T
b_2	-0.004	-6.194	0.004
b_3	0.014	-3.215	0.002
b_4	0.041	-1.256	0.035
b_5	-0.069	-0.480	-0.060

	Layout 1		Layout 2
b_6	-0.031	-0.122	-0.030
b_7	0.100	0.088	0.111
b_8	0.174	0.177	0.176
b_9	-0.469	-0.484	-0.483
b_{10}	-0.274	-0.283	-0.305
b_{11}	1.407	1.450	1.471
b_{12}	-1.509	-1.555	-1.524
b_{13}	0.588	0.606	0.645
b_{14}	0.098	0.101	0.147
b_{15}	-1.587	-1.634	-1.636

The coil block parameters for layout 2 are given in Table 17. Compared to layout 1 optimized at 3.5 T (Table 11), the most significant change is the increase of the positioning angle of coil block 15 by 0.245 degrees.

Table 17 Coil block parameters for the first and second quadrant in the right aperture for layout 2 optimized at 4.5 T. The block number definition is given in Figure 2.

Block	Number of cables	Positioning angle (degree)	Inclination angle (degree)
1	11	2.0806	0.9
2	8	25.413	24.5
3	4	44.178	42.5
4	4	57.407	55.7
5	2	76.803	73.97
11	12	0.5650	0
12	8	24.087	24.5
13	4	42.660	42.5
14	4	58.085	55.7
15	1	80.736	73.97

At the nominal current 13850 A, the bore field is 4.506 T and the peak field in the coil is 5.306 T. This gives a ratio of 1.178. The load-line is plotted in Figure 20. The maximum load line working point is 70%.

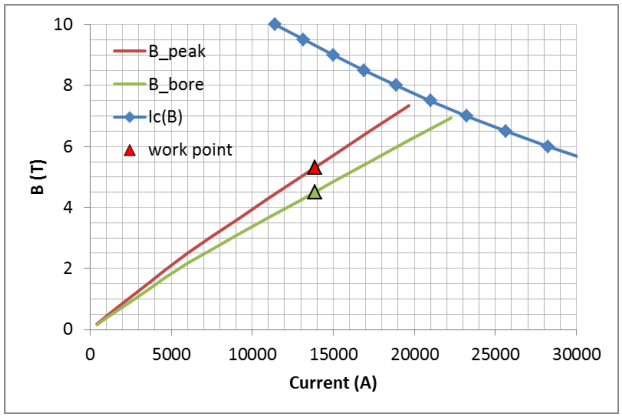

Figure 20 Load line for the coil layout optimized at 4.5 T. The maximum load line working point is 70%.

9.2 Fringe field

At 4.5 T main field, the fringe field at R = 501 mm ranges from 45 to 105 mT at 4.5 T (Figure 21), higher than the 20 mT level.

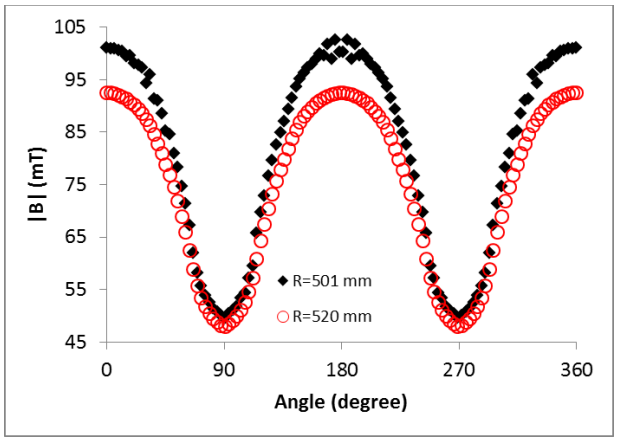

Figure 21 Fringe field with the main field of 4.5 T. Yoke OD = 560 mm, shell thickness = 10 mm.

The parametric study with different values for yoke OD and shell thickness is shown in Figure 22. Again, a yoke optimization beyond the simple window-frame considered for this study is expected to yield improved performance in terms of maximum field/operating margin, field quality and fringe field characteristics.

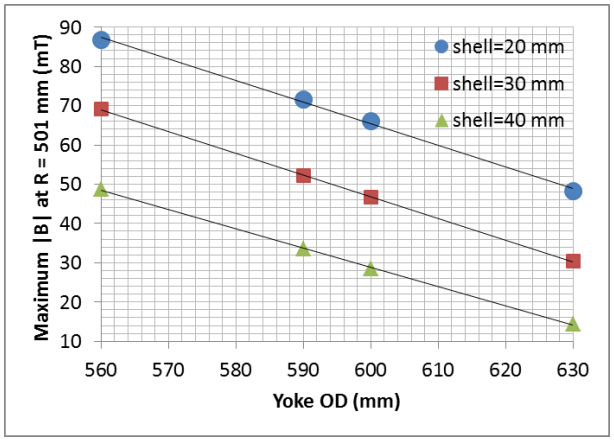

Figure 22 Maximum fringe field at R = 501 mm with different shell thickness and yoke OD at main field of 4.5 T. Solid lines are linear fits of the data points.

10 Conclusions

The recombination dipole magnet is required to be upgraded for the High-Luminosity LHC project. The main design challenge for this magnet is to decouple the magnetic field in the two apertures and ensure good field quality. An approach to achieve this is summarized in this report. The iron yoke is designed primarily for low saturation effects, and the resulting large but current-independent cross-talk between the apertures is corrected with an asymmetric arrangement of the conductor blocks. A design study based on the LHC dipole cable is performed. The expected field harmonics for geometric, saturation and persistent current effects are given and compared to the latest error table (version 1.4, 2013). The fringe field as a function of the outer diameter of the iron yoke is also presented. The feasibility of increasing the operating field from 3.5 T to 4.5 T, with the magnetic length decreasing from 10 m to 7.8 m, was discussed.

A yoke optimization beyond the simple window-frame considered for this study is expected to yield improved performance in terms of maximum field/operating margin, field quality and fringe field characteristics.

11 Appendix: strand and cable parameters

The LHC main dipole (MB) outer layer cable is considered in this report. The cable data is from the Roxie cable database (cable name “YELLONOU”). The main parameters for the conductor and cable are listed in Table 18 and Table 19.

Table 18 Parameters for the Nb-Ti filament and strand.

Item	Unit	Value
Nb-Ti Filament diameter	μm	6
Strand diameter	mm	0.828
Cu/SC ratio	-	1.9
RRR	-	80
J_c (1.9 K, 5 T)	A/mm^2	1953

Table 19 Parameters for the Nb-Ti cable.

Item	Unit	Value
Height	mm	15.1
Minor edge width	mm	1.362
Major edge width	mm	1.598
Radial side insulation thickness	mm	0.15
Azimuthal side insulation thickness	mm	0.13
Number of strands	-	36
Pitch length	mm	100

12 Appendix: multipole change during coil block design

The multipole change at various steps of coil block design is shown in Table 20. Geometric and saturation effects are considered. The normal harmonics in the left aperture have the same magnitude as listed with opposite polarity for even-order terms. The skew terms in both apertures are zero.

Table 20 The computed normal harmonics in the right aperture at 10300 A with the cross section determined by selected steps, R_{ref} = 35 mm.

	Unit	Initial layout (Step 0)	After removing turns (Step 2)	After adjusting coil block positions (Step 6)	With the yoke half height of 120 mm (Step 8)	Phi2 25.2 → 25.3 deg, 23.8 → 23.7 deg (same block in step 5)	Roxie optimization
Current	A	9500	10300	10300	10300	10300	10500
B_1	T	3.4831	3.5273	3.5189	3.5469	3.5468	3.5453
b_2	unit	240.783	27.402	-41.545	-19.730	-24.760	-0.004
b_3		-207.097	-17.512	0.655	0.920	0.823	0.014
b_4		36.937	22.663	2.625	2.818	-0.352	0.041
b_5		48.859	-25.991	7.478	-3.053	-2.907	-0.069
b_6		1.841	-14.490	0.110	0.106	0.390	-0.031
b_7		6.220	4.850	4.811	-0.366	-0.275	0.100
b_8		0.069	-6.665	-1.493	-1.478	-0.606	0.174
b_9		6.082	-2.011	0.950	-1.174	-1.188	-0.469
b_{10}		0.004	-0.511	-1.340	-1.337	-1.052	-0.274
b_{11}		-0.559	0.868	3.801	3.179	3.146	1.407
b_{12}		0.000	-1.399	-1.484	-1.490	-1.535	-1.509
b_{13}		0.554	0.394	-0.109	-0.258	-0.268	0.588
b_{14}		0.000	0.012	0.112	0.118	0.058	0.098
b_{15}		-0.235	-1.116	-1.155	-1.185	-1.182	-1.587

13 References

[Bellesia06]. B. Bellesia and E. Todesco, Random Errors in Superconducting Dipoles, in Proceedings of EPAC 2006. https://accelconf.web.cern.ch/accelconf/e06/PAPERS/WEPLS097.PDF

[Bottura02] L. Bottura, A Practical Fit for the Critical Surface of NbTi. IEEE Trans. Appl. Supercond., 10(1), 2002, pp. 1054 – 1057.

[Brüning04] O. S. Brüning, P. Collier, P. Lebrun, S. Myers, R. Ostojic, J. Poole, and P. Proudlock, Eds., LHC Design Report. Geneva: CERN, 2004, vol. 1, ch. 8, pp. 230–234.

[De Maria13] R. De Maria, S. Fartoukh, A. Bogomyagkov, and M. Korostelev, "HLLHCV1.0: HL-LHC layout and optics models for 150mmNb3Sn triplets and local crab-cavities", in Proceedings of IPAC'13, Shanghai, May 2013, pp. 1358–1360, http://www.JACoW.org

[Ferracin00] P. Ferracin *et al.*, Modeling of Random Geometric Errors in Superconducting magnets with Applications to the CERN Large Hadron Collider, Physical Review ST Accelerators and Beams, 3, 122403, 2000.

[Gupta13] R. Gupta, Conceptual Magnetic Design of 105 mm Aperture Dipole D2. Presentation at CM20, 10 April 2013.
https://indico.fnal.gov/getFile.py/access?contribId=68&sessionId=8&resId=0&materialId=slides&confId=6164

[Jain98] A. K. Jain, "Basic theory of magnets," in CERN Accel. School, Meas. Alignment Accel. Detect. Magn., 1998, pp. 1–26, CERN-98-05.

[Nakamoto04] T. Nakamoto *et al.*, Design of Superconducting Combined Function Magnets for the 50 GeV Proton Beam Line for the J-PARC Neutrino Experiment, IEEE Trans. Appl. Supercond., 14(2), 2004, pp. 616.

[Redaelli00] S. Redaelli, Analysis of the Magnetic Field Perturbations in Dipoles and Quadrupoles of the Large Hadron Collider (LHC), Ph.D. thesis, The University of Milan (2000).

[Russenschuck10] S. Russenschuck, Field Computation for Accelerator Magnets: Analytical and Numerical Methods for Electromagnetic Design and Optimization. Hoboken, NJ, USA: Wiley, 2010.

[Sabbi13] G. Sabbi, "D2 conceptual design, status and next steps", presentation at High Luminosity LHC Annual Meeting, Daresbury, UK, November 11-14, 2013.
https://indico.cern.ch/getFile.py/access?contribId=76&sessionId=21&resId=0&materialId=slides&confId=257368

[Todesco13] E. Todesco, D2 field error tentative table, presentation at WP3 meeting, 22 October 2013.
https://lhc-div-mms.web.cern.ch/lhc-div-mms/tests/MAG/docum/hilumi/Presentations/2013-10-22_et_D2_fq_1013.pptx

See also https://lhc-div-mms.web.cern.ch/lhc-div-mms/tests/MAG/docum/hilumi/Magnets/field_quality.xlsx

[Todesco14] E. Todesco, H. Allain, G. Ambrosio, G. Arduini, F. Cerutti, R. De Maria, L. Esposito, S. Fartoukh, P. Ferracin, H. Felice, R. Gupta, R. Kersevan, N. Mokhov, T. Nakamoto, I. Rakno, J. M. Rifflet, L. Rossi, G. L. Sabbi, M. Segreti, F. Toral, Q. Xu, P. Wanderer, and R. van Weelderen, A First Baseline for the Magnets in the High Luminosity LHC Insertion Regions, IEEE Trans. Appl. Supercond., 24(3), 4003305, 2014.

[Völlinger02] Christine Völlinger, Superconductor Magnetization Modeling for the Numerical Calculation of Field Errors in Accelerator Magnets, PhD Thesis, Technical University of Berlin, 2002.

[Willen00] E. Willen, M. Anerella, J. Cozzolino, G. Ganetis, A. Ghosh, R. Gupta, M. Harrison, A. Jain, A. Marone, J. Muratore, S. Plate, J. Schmalzle, P. Wanderer, and K. C. Wu, "Superconducting dipole magnets for the LHC insertion regions", in Proceedings of EPAC'00, Vienna, June 2000, pp. 2187–2189, http://www.JACoW.org

[WP3] E. Todesco, https://espace.cern.ch/HiLumi/WP3/SitePages/Home.aspx

[Xu14] Q. Xu, Tatsushi Nakamoto, Masami Iio, Toru Ogitsu, Kenichi Sasaki, Akira Yamamoto, Ezio Todesco, and Bernhard Auchmann, Design Optimization of the New D1 Dipole for HL-LHC Upgrade, IEEE Trans. Appl. Supercond., 24(3), 4000104, 2014.